ACS NANO

www.acsnano.org

ARTICLE

Macroscale Superlubricity Induced by MXene/MoS_2 Nanocomposites on Rough Steel Surfaces under High Contact Stresses

Ali Macknojia, Aditya Ayyagari,* Dario Zambrano, Andreas Rosenkranz, Elena V. Shevchenko, and Diana Berman*

Cite This: *ACS Nano* 2023, 17, 2421−2430

Read Online

ACCESS | Metrics & More | Article Recommendations | Supporting Information

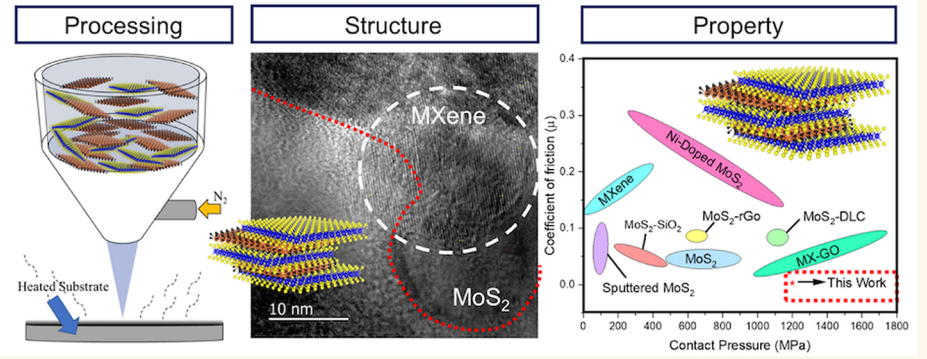

ABSTRACT: **Toward the goal of achieving superlubricity, or near-zero friction, in industrially relevant material systems, solution-processed multilayer $Ti_3C_2T_x$-MoS_2 blends are spray-coated onto rough 52100-grade steel surfaces as a solid lubricant. The tribological performance was assessed in a ball-on-disk configuration in a unidirectional sliding mode. The test results indicate that $Ti_3C_2T_x$-MoS_2 nanocomposites led to superlubricious states, which has hitherto been unreported for both individual pristine materials, MoS_2 and $Ti_3C_2T_x$, under macroscale sliding conditions, indicating a synergistic mechanism enabling the superlative performance. The processing, structure, and property correlation were studied to understand the underlying phenomena. Raman spectroscopy, scanning electron microscopy, and transmission electron microscopy revealed the formation of an *in situ* robust tribolayer that was responsible for the performance at high contact pressures (>1.1 GPa) and sliding speeds (0.1 m/s). This report presents the lowest friction obtained by either MoS_2 or MXene or any combination of the two so far.**

KEYWORDS: *superlubricity, MXenes, molybdenum disulfide, steel, friction, wear, solid lubrication*

Identifying materials and systems that can render superlubricity in real-world applications is an important research area in sliding mechanical systems.[1] Several niche applications call for oil-free lubrication that can benefit from nearly frictionless sliding on multiasperity contacts, also known as engineering rough surfaces (ERS). Graphene,[2−6] nanodiamonds,[7,8] and their combinations[9,10] have been shown to induce superlubricity. However, it must be pointed out that this phenomenon has been reliably observed in a limited range of controlled systems: namely, with an inert counterface like diamond-like carbon (DLC), using atomically smooth substrates such as silica wafers, or under vacuum conditions.[11−16] Other 2D materials, such as MoS_2 and graphene oxide, are known to be promising solid lubricant materials, but the superlubricity in those has been dependent on the material alignment and is highly sensitive to atmospheric conditions and materials purity. Martin et al.[12,13,17] have attributed the mechanisms in the lubricity of MoS_2 to intragranular shear and intercrystallite slip, both of which are closely related to the individual crystal rotation/orientation. Importantly, the lubricity properties have been attributed to (a) intrinsic material properties of MoS_2 flakes in the aforementioned

Received: September 27, 2022
Accepted: December 20, 2022
Published: January 25, 2023

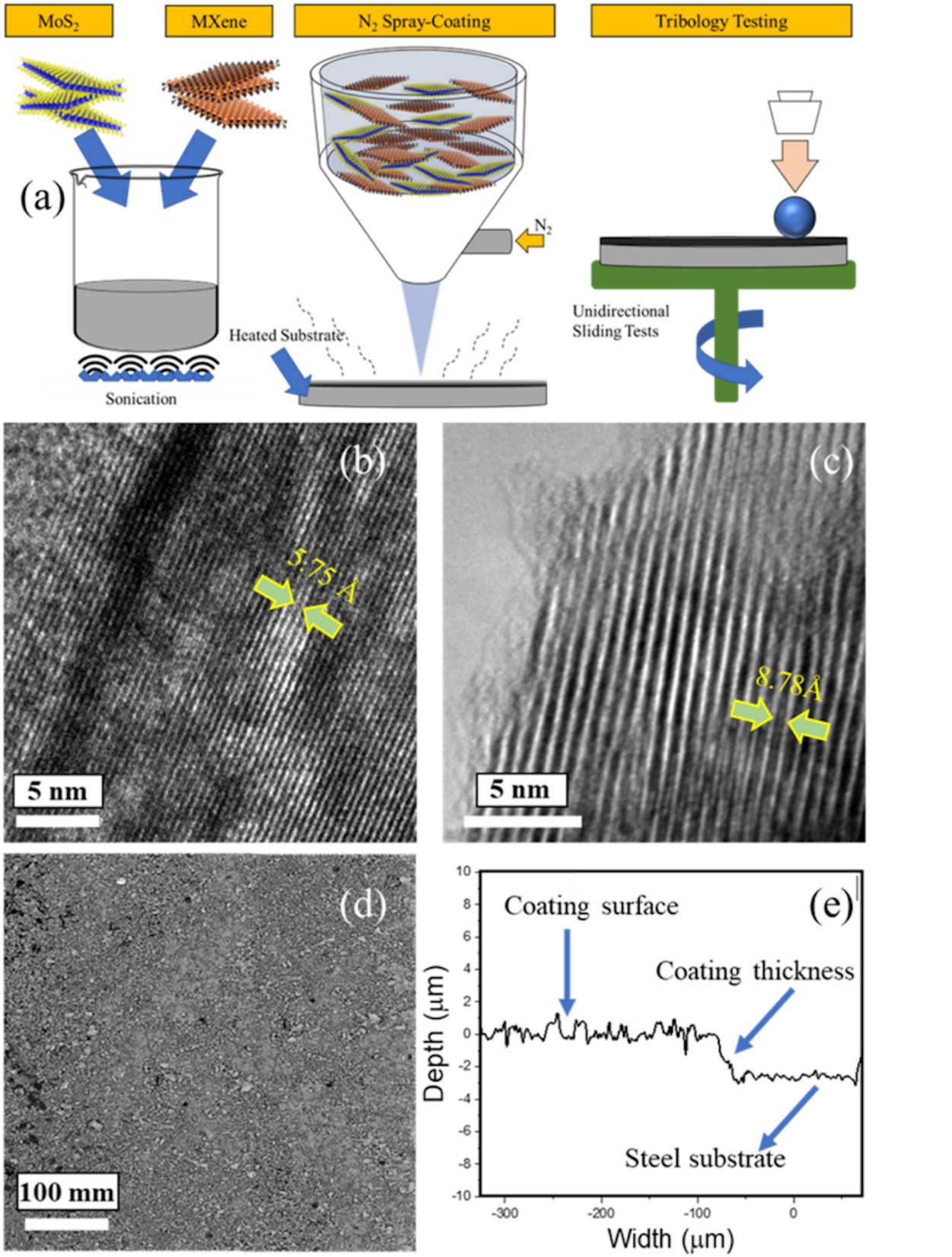

Figure 1. Schematic illustration showing the generation of suspensions containing solid lubricants in a nonreactive carrier medium (ethyl alcohol) nd subsequent spray coating onto the preheated substrate, as well as unidirectional ball-on-disk sliding experiments. High-resolution TEM images showing the lattice spacings of (b) MoS_2 as 5.75 Å and (c) $Ti_3C_2T_x$ as 8.78 Å. (d) Light microscopic image of the coated steel substrate (e) with the corresponding surface profile showing the coating thickness of the solid lubricant deposited onto an AISI 52100 steel substrate. The average coating thickness was 3.3 ± 0.1 μm, and the roughness of the coated substrates was 450 ± 50 nm.

https://doi.org/10.1021/acsnano.2c09640
ACS Nano 2023, 17, 2421−2430

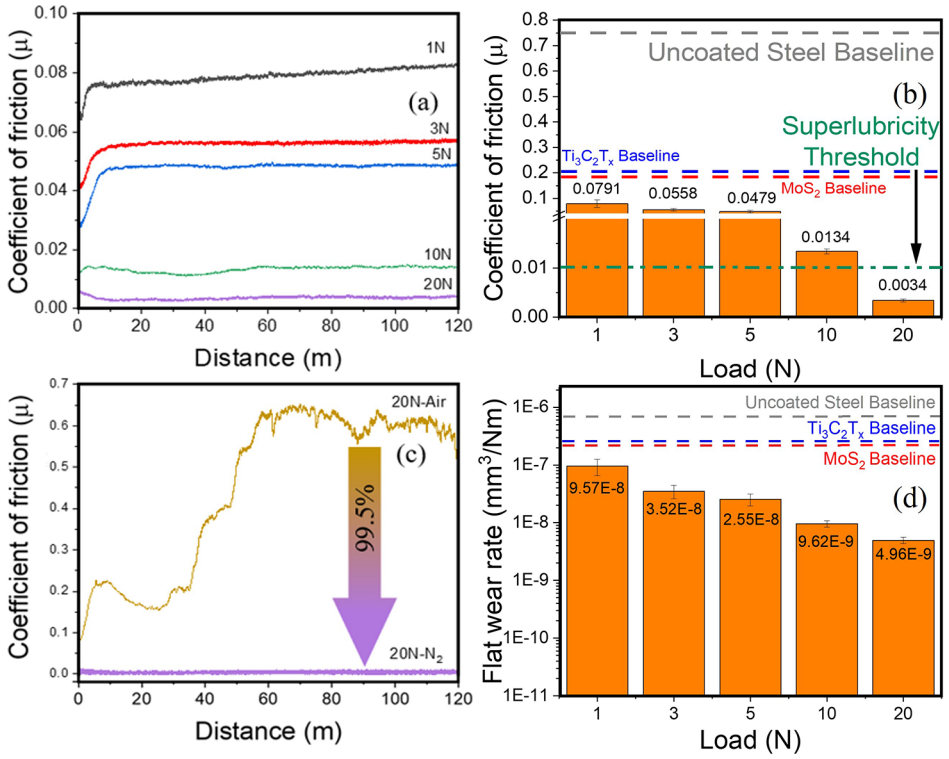

Figure 2. (a) Coefficient of friction behavior showing the performance of MoS_2-$Ti_3C_2T_x$ solid lubricant coatings under unidirectional sliding at 0.1 m/s under various contact loads as a function of sliding distance in dry nitrogen. (b) Summary of steady-state friction values juxtaposed with steel-on-steel, MoS_2-on-steel, and $Ti_3C_2T_x$ -on-steel references. (c) Coefficient of friction measured at 20 N and 0.1 m/s under ambient conditions in contrast with the friction at 20 N under dry nitrogen conditions, showing the effect of humidity on the tribological performance. (d) Coating wear on the steel substrate as a function of the normal load after sliding for the same distance. The friction was observed to decrease with an increase in the normal load (contact pressure), with the 20 N test condition surpassing the superlubricity threshold by 1 order of magnitude (0.0034). Wear rates were observed to decrease with increasing load as was the case for friction.

orientations, rather than contact mechanics conditions, (b) orientation of the grains, or basal plane reorientation, and (c) intragranular and intercrystalline shear in the MoS_2 grains.[12,13,17] The major limitation for the advancement is that most 2D materials call for highly controlled processing steps such as atomic layer deposition, physical or chemical vapor deposition, or sputtering that invariably need high-vacuum systems, thus presenting limitations of size, geometry, and uniformity.[18]

Slip and/or shear between the atomic planes in layered structures such as in graphite,[19] graphene,[20,21] graphene oxide,[22] MoS_2,[17,23−25] and WS_2,[26−29] among others, are primarily responsible for lubricity in solid-state sliding. The tribomechanical or chemical phenomena such as crumbling of the layered structure under high contact pressure,[30] reactions between the substrate and coating material changing its chemical/crystal structure,[31−33] or materials degradation by intercalation with impurities,[17] oxygen, or water molecules (also referred to as structural water)[34] are generally attributed to the loss of lubricity over prolonged sliding and are barriers to realizing superior performance. Therefore, the search for more reliable and tribologically effective material systems continues.

MXenes are a class of layered materials that could potentially overcome these drawbacks, as they offer flexibility in the structure and composition beyond previously tested 2D materials while providing the lubrication benefits of the layered materials. MXenes have been explored for their tribological properties[35,36] as lubricant additives in oils[37,38] and organic solvents[39,40] and as reinforcements in polymer-based composites[41−45] and solid lubricants.[46−48] MXenes have been shown previously to provide a superlubricity regime when they are deposited on an atomically flat silicon substrate and tested against the DLC surface.[48] However, there are no reports that have demonstrated a prolonged, sustainable superlubrication performance when they are used as a solid-state lubricant reducer on ERS with a steel counterface. To bridge this knowledge gap, we demonstrate the pathways for achieving superlubricity on ERS ($R_a \approx 200$ nm) multiasperity contacts, using hybrid $Ti_3C_2T_x$-MoS_2 coatings.

This paper reports a simple spray-coating process for the deposition of hybrid $Ti_3C_2T_x$-MoS_2 coatings that resulted in an exceptional lubricity performance under dry conditions under high contact pressures of ~1.1 GPa. The detailed characterization of the tribological interface revealed the origin of such superlubricity in the rearrangement of the 2D materials to accommodate the applied stresses. Optical profilometry, scanning electron microscopy, transmission electron microscopy, Raman and X-ray photoelectron spectroscopy, and nanoindentation were used to quantify the properties and delineate the phenomenon. Our findings unravel opportunities for frictionless sliding systems operating under conditions relevant to industrial applications.

https://doi.org/10.1021/acsnano.2c09640
ACS Nano 2023, 17, 2421−2430

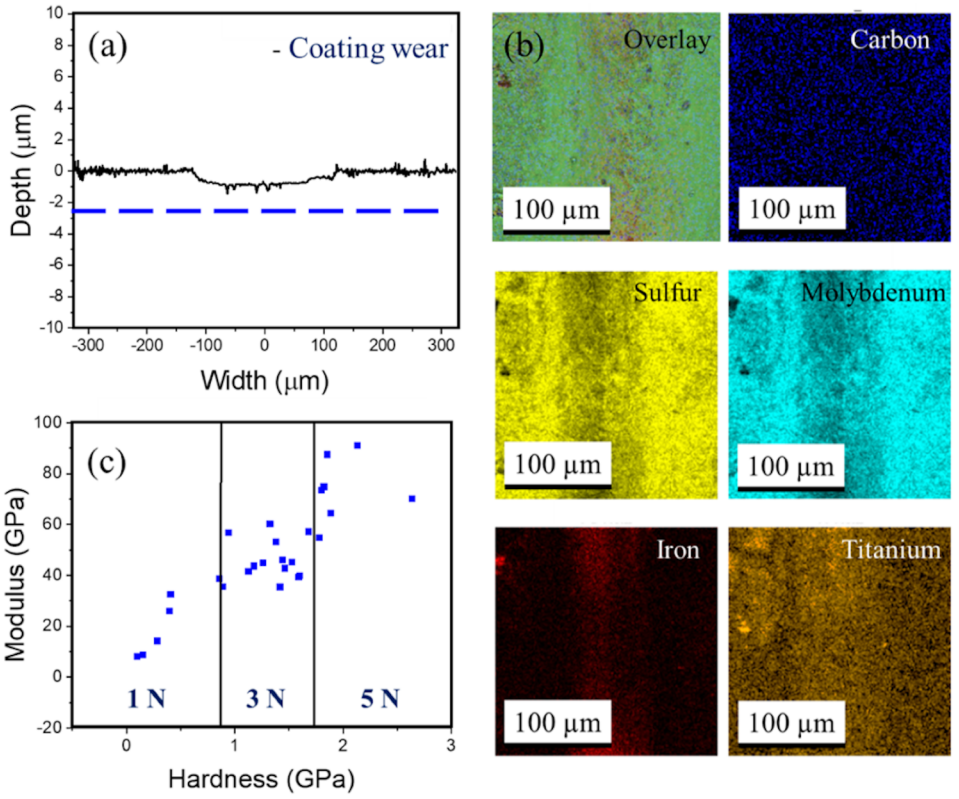

Figure 3. (a) Surface profile of the wear track of the hybrid nanocomposite at 20 N. (b) SEM-EDS mapping showing the distribution of elements on the coating and wear track. (c) Summary of the results obtained by nanoindentation analysis inside the formed wear tracks showing an increasing hardness and modulus with sliding across test loads.

RESULTS AND DISCUSSION

A schematic illustration of the coating process and tribological testing in unidirectional sliding is shown in Figure 1a. The composition of the coating has been optimized to reveal the maximum lubricity potential of the materials (Supporting Information).

High-resolution TEM micrographs of the pristine as-received MoS_2 and $Ti_3C_2T_x$ (T_x indicates the surface terminations of the outer metal layers in the MXene structure, such as O, OH, etc.) are shown in Figure 1b,c, respectively. Both materials had a microcrystalline size (up to 500 nm length and width), and multiple-layer (up to 30−50 layers for MoS_2 and up to 50−60 layers for $Ti_3C_2T_x$) structures. The lattice parameters of MoS_2 and $Ti_3C_2T_x$ were about 5.75 and 8.78 Å, respectively, as calculated from Figure 1b,c. An SEM image of the as-deposited coating is shown in Figure 1d. The roughness of the coated substrates was 450 ± 50 nm. The coating thickness was measured by removing the deposited material with a sharp scribe and measuring the step height between the underlying steel substrate and the top surface. This procedure was repeated at multiple locations on each substrate, thus calculating a coating thickness of 3.1 ± 0.1 μm as shown in Figure 1e.

Friction data for individual test conditions are shown in Figure 2, while the average steady-state friction values are shown in Figure 2b. The coefficients of friction of the steel-against-steel, MoS_2-on-steel, and $Ti_3C_2T_x$ -on-steel benchmarking tests, performed with a 1 N load, were 0.78, 0.19, and 0.2, respectively. Higher load benchmarking was successful only for the MoS_2-on-steel system for loads up to 5 N (Figure S1), since for all other samples the peak friction triggered the autocutoff on the tribometer and terminated the tests immediately after the break-in.

Coefficient of friction data for hybrid composites showed that friction reduced by 89% in the 1 N test to 0.0791, by 91% in the 3 N test to 0.055, by 94% in the 5 N test to 0.047, by 2 orders of magnitude to 0.013 at 10 N, and surpassing the superlubricity threshold (of 0.01) by 1 order of magnitude at 20 N with a friction of 0.0034. Each test was repeated at least three times to confirm the measurements. The best test conditions, namely 20 N and 0.2 m/s sliding, was run for 2 h totaling 40000 cycles (1.2 km), demonstrating steady-state friction at 0.003, which confirmed the materials' performance to be prolonged and repeatable. Figure 2c shows the friction results on sliding under humid conditions (RH 42%), with values reaching as high as 0.65. This, in comparison with the test results from dry nitrogen sliding, clearly shows the deleterious effects of environmental oxygen and/or water vapor. Following ascertaining friction response and its repeatability, the wear induced on the coated surfaces was studied, and the results are presented in Figure 2d (and in Figure S2). The results indicate a 2 orders of magnitude reduction in the wear rate for the coating tested at a 20 N load in comparison to the bare steel vs steel sliding at 2 N and 0.1 m/s. A representative surface profile of the wear track is shown in Figure 3a. The depth of the wear track was about 0.7−0.8 μm for the 20 N 0.1 m/s test condition and was much shallower for lower loads. These results suggest that the coating still remained intact during sliding and its compression and adaptation allowed reducing the effect of the steel substrate roughness on the frictional behavior. The modified materials in the wear track also exhibited strong adhesion to

https://doi.org/10.1021/acsnano.2c09640
ACS Nano 2023, 17, 2421−2430

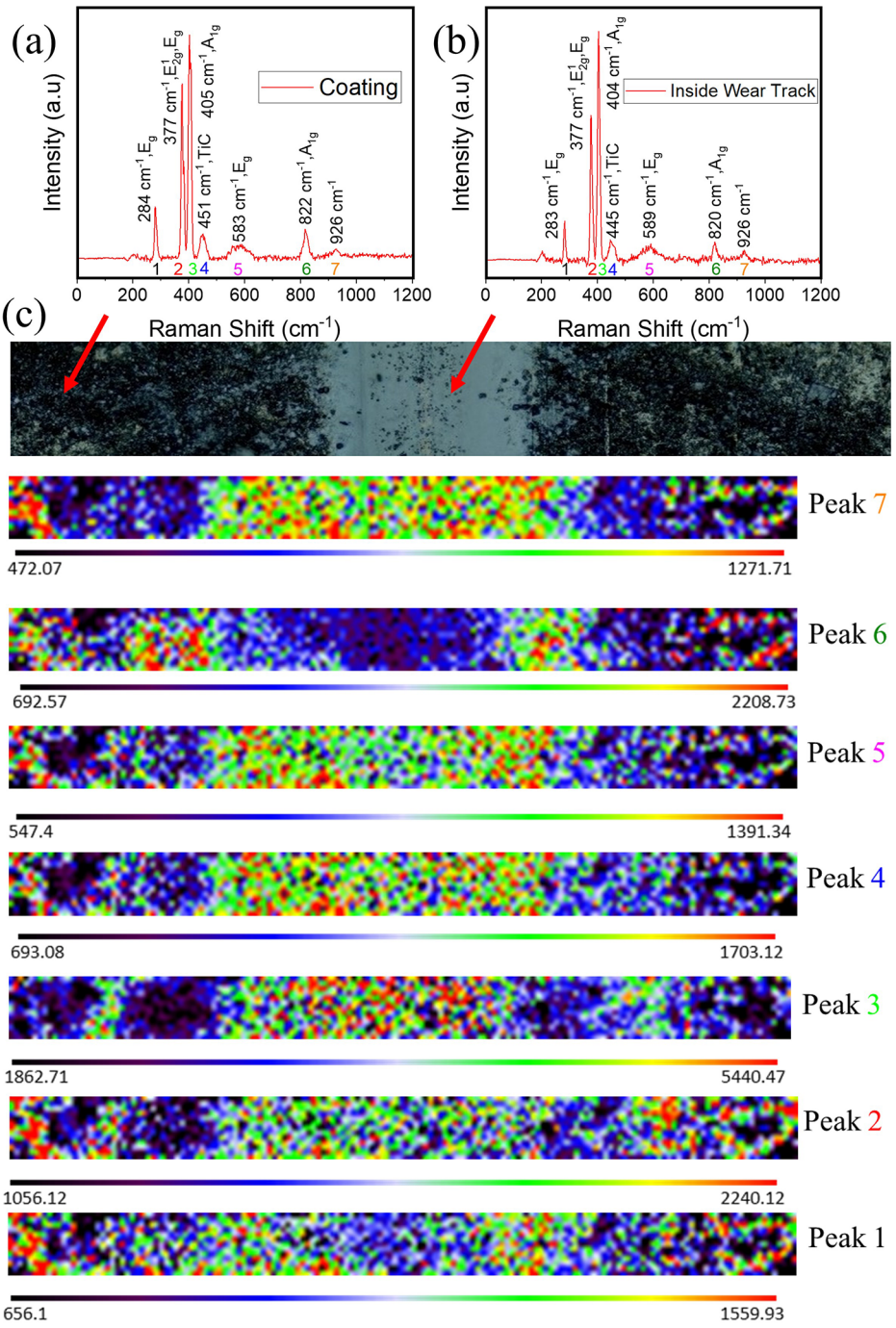

Figure 4. Raman spectra acquired on (a) as-deposited hybrid coating and (b) inside the wear track after tribological testing. (c) Raman mapping on the wear track. The data shown here correspond to the wear track generated for a normal load of 20 N.

the substrate that made them capable of sustaining high load and shear stresses.

The coating inside the sliding path remained intact at the end of the sliding experiments, both short-term and long-term, and did not reveal the underlying steel in any of the test cases. A representative elemental mapping for the extreme test condition, namely 20 N, is shown in Figure 3b. The faint Fe signal is expected to originate from the underlying, unexposed steel substrate due to the depth of electron material interactions. The entire wear on the surface seen as deformation/compression of the hybrid coating was contained within the thickness of the deposit. The sliding path was brighter than the as-deposited coating, indicating that the coating may have been slightly polished during sliding.

To quantify the changes in the mechanical properties of the coating material during sliding and to understand the mechanisms resulting in superlubricity, nanoindentation experiments were carried out inside the formed wear tracks for all sliding conditions. The corresponding results are shown in Figure 3c. A clear trend of increasing the resistance to indentation and stiffness was seen with increasing contact pressure. The indentation data are presented up to 5 N, since during the tests performed at 10 and 20 N the depth of the wear tracks approaches the thickness of the coating and thus

https://doi.org/10.1021/acsnano.2c09640
ACS Nano 2023, 17, 2421−2430

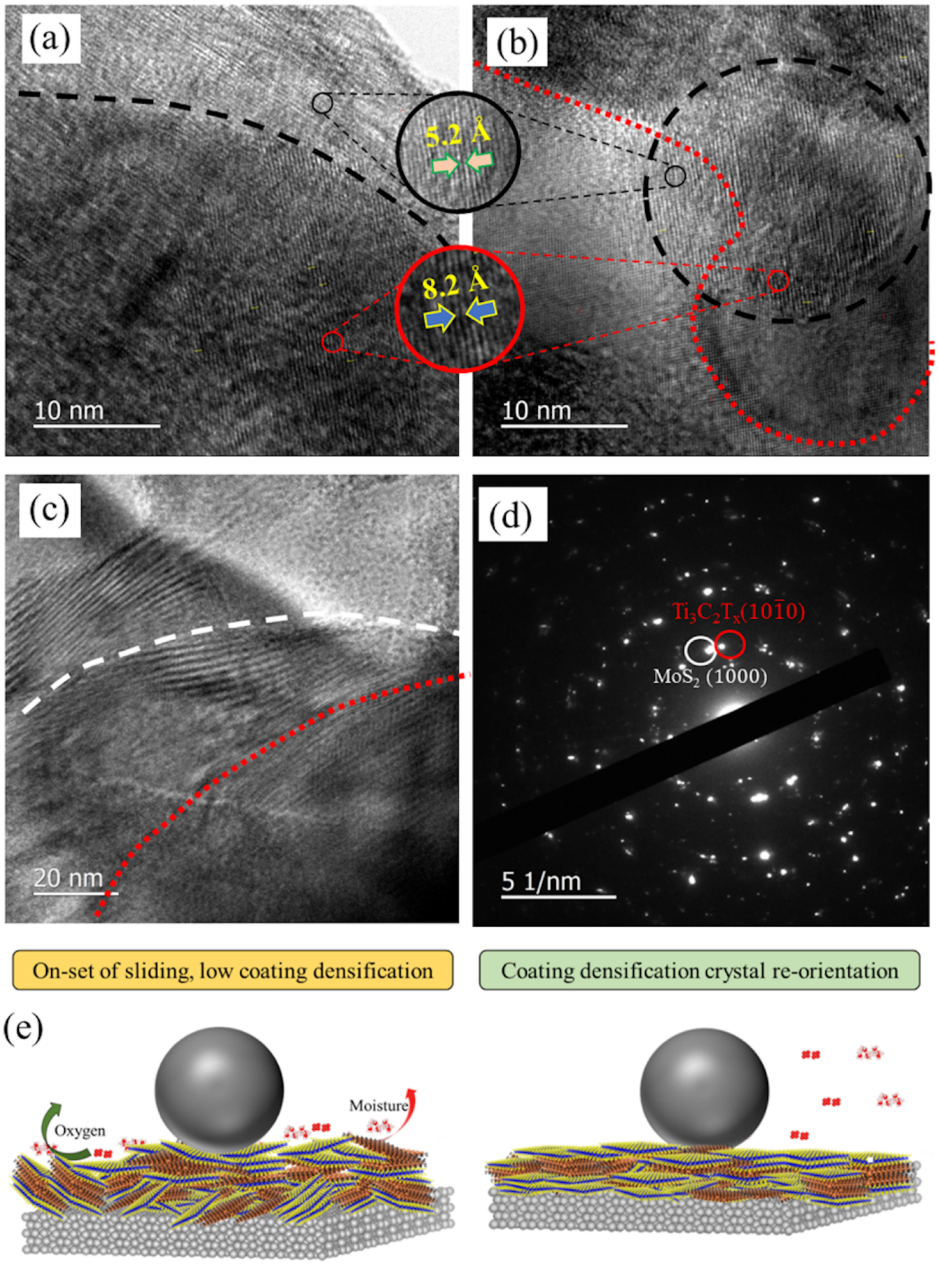

Figure 5. Bright-field TEM images of the tribolayer at (a) the 10 N test showing composite MXene and MoS_2 overlapped flakes, (b) the 20 N short-term test, and (c) the end of the long-term test. (d) Electron diffraction image. (e) Schematic of an in-*operando* mechanism consisting of coating densification and reorientation that resulted in superlubricity.

the steel substrate largely affects the measurements of the hardness and the elastic modulus. Indeed, the measured hardness values for 10 and 20 N wear tracks were measured to be 6.5 and 6.6 GPa respectively, which is close to the 6.6 GPa hardness of the steel substrate. The observed trend of the hardness and elastic modulus increase as a function of the load at which the tribotests were performed is unambiguous evidence of a compaction-driven increase in hardness and modulus that has improved the lubricity, thus preventing a steel-on-steel contact and improving the respective wear resistance. The surface of the tribological counterbody studied by optical profilometry and scanning electron microscopy does not indicate any pronounced wear but did show firm adherence of the transfer layer that could not be removed by wiping or sonication (to assess ball cap diameter). The nanoindentation results and wear data, from both the substrate and counterface ball, indicate that there is an absence of wear loss of the steel surfaces; sliding at high contact pressures resulted in compaction and densification of the coating that resulted in a robust tribofilm, which prevented the direct steel-on-steel contact. This mechanical phenomenon in combination with the shearing of the layered materials within the tribofilm contributed to the sustained superlubricity. The densification phenomenon is consistent with previous reports by Mogne et al., where very dense, hard coatings were observed to produce exceptional lubricity.[13]

To further probe the origin of the observed superior lubricity, structural (crystallographic and morphological) and compositional (chemical bonding) changes in the coating were evaluated. Figure 4 summarizes the spectra collected from the

https://doi.org/10.1021/acsnano.2c09640
ACS Nano 2023, 17, 2421−2430

(center of) wear track formed during superlubric sliding under 20 N test conditions in comparison to a representative Raman spectrum acquired on the as-deposited hybrid coating. A gradual transition in the Raman signal is observed across the regions of the sliding path. The tribotests induced changes in the characteristic peaks of the as-deposited, pristine $Ti_3C_2T_x$-MoS_2 nanocomposite at 284 ($Ti_3C_2T_x$), 377 (E^1_{2g} and $Ti_3C_2T_x$), 406 (A_{1g}), 598 (E^1_{2g} + LA), and 822 cm^{-1} ($2A_{1g}$), while the intensity of the peaks located at 379 and 406 cm^{-1} remained unchanged. The intensities of the E^1_{2g} and A_{1g} peaks were higher compared to those of the as-deposited coating, indicating that the structure of MoS_2 experienced a basal plane reorientation of the basal planes under shearing and compressive loads. The MXene component of the nanocomposite did not produce any resolvable spectral signal in the sliding path due to signal-drowning from the MoS_2. A faint peak at 820 cm^{-1} was noticed in the as-deposited coating, which was observed to be absent inside the wear track, and none of the spectra had 159 or 666 cm^{-1} peaks. These three peaks, namely, 159, 666, and 820 cm^{-1}, correspond to MoO_3[49] and may indicate a complete absence of oxidation/oxide formation during the wear testing. 2D maps of all the major Raman peaks (Figure 4c) indicate the consistency of the coating inside the wear track. Interestingly, an analysis of the steel counterpart after sliding (Figure S3) indicates transfer of the coating to the ball side to ensure easier shearing of materials with no signs of the steel substrate wear. In stark contrast, the Raman analysis of the wear track produced in a humid environment (Figure S4) shows no coating presence inside the wear track after the sliding.

The X-ray photoelectron spectra (presented in Figure S5) for the as-deposited coating and inside the wear track formed during superlubric sliding summarize the changes in the Mo_{3d}, Ti_{2p}, and S_{2p} peak regions. The peak deconvolution of the Mo_{3d} region indicates a decrease of the Mo^{6+} oxidation state with sliding. This corroborates the results obtained by Raman spectroscopy and affirms the understanding that there is an elimination of MoO_3. The formation of MoO_3 is a known mechanism of dangling bond saturation in MoS_2[49−52] when crystal degradation or disruption occurs during sliding and has been extensively documented to deteriorate the lubricity performance.[25,30−33] This brings up the question as to why an indication of oxide was observed in the starting materials/pristine coating and not in the tribolayer. This could be attributed to two plausible sources. On the one hand, the exposure to ambient conditions and adsorption of oxygen may have led to the oxidation of MoS_2 crystallites at defect sites or edges. On the other hand, it may be traced back to potential oxidation from the residual oxygen from the ethanol-based deposition procedure. Continuous purging of nitrogen at low dew-point temperature combined with tribochemical reactions and reorientation might be responsible for the observed decrease/vanishing of the oxygen. Additionally, Ti, which may be released from Ti_3C_2Tx during sliding, is a known oxygen absorber and its presence may accelerate the removal of the adsorbed oxygen from MoS_2.[51,52] It is hypothesized that the synergistic mechanism wherein deleterious effects are eliminated by local transfer of oxygen/structural water from one constituent phase to another effectively resulted in vanishing friction for unlimited lubricity. To explain the phenomenon by quantifying microstructural changes, small scraps of the tribolayer were mounted onto copper grids for transmission electron microscopy. The bright-field TEM images and electron diffraction patterns are shown in Figure 5.

The TEM micrographs depicted in Figure 5a show the two materials with distinct lattice spacings overlapping each other with MoS_2 flakes extending beyond the phase mixture, delineated with the black dotted line. Similar microstructural features can be seen in Figure 5b,c, respectively, wherein darker multilayer regions with both MoS_2 and $Ti_3C_2T_x$ were interspersed in larger MoS_2 blankets, as shown with the white and red dotted lines, respectively. The three bright-field images, albeit from different test and load conditions, retain significant similarities to that of the pristine, as-received materials as shown in Figure 1, indicating no flake-/crystal-level deformation of lattice disruption. Figure 5d (and Figure S6) shows a representative electron diffraction (ED) image from the phase mixture ,showing bright diffraction spots from both crystals and a complete absence of halos, smearing, and formation of continuous or discrete rings across multiple analysis regions. This confirms that the phases retained their high degree of crystallinity with no significant degradation of MoS_2 or $Ti_3C_2T_x$ whatsoever. Moreover, there was no formation of amorphous phases that are typically observed to form in high-load, high-speed sliding of 2D materials.[26,30]

The data from white light interferometry, scanning electron microscopy with energy dispersive X-ray spectroscopy, nanoindentation, Raman spectroscopy, and X-ray photoelectron spectroscopy, supported by bright-field transmission electron microscopy and electron diffraction imaging, converge to the following observations: a robust tribolayer was formed and continually hardened (driven by compaction and densification) during sliding. The tribolayer was thick and resilient to accommodate deformation from high contact pressure and prevented direct (steel-on-steel) contact between the sliding tribopairs. By virtue of sliding under a dry nitrogen atmosphere, and the relative affinity of Ti to oxygen, the deleterious effects of oxygen or structural water intercalation on the lubricity behavior of MoS_2 and $Ti_3C_2T_x$ could be completely circumvented to provide ultralow, stable, prolonged superlubricity. An increased signal strength from the basal planes of MoS_2, which indicates the reorientation of the MoS_2 crystallites in the tribolayer, and $Ti_3C_2T_x$ form the structural truss that facilitated hitherto unseen exceptional lubricity performance under dry conditions. The respective mechanisms are illustrated in the schematics shown in Figure 5e.

The observed lubricity results were significantly lower compared to those of previously reported coatings deposited using similar technologies such as burnished or (magnetron, rf) sputtered MoS_2 under dry, ambient, and humid sliding conditions. The results also outperform composite and chameleon coatings, MoS_2 doped or blended with other materials such as gold, silica, nickel, graphene, and graphene oxide, MXenes, and MXene blends and even in comparison to oil- or liquid-based lubrication with MXene[1] or MoS_2 additives as illustrated in the Ashby plot shown in Figure 6.[22,23,30−33,36,46,47,53−57]

CONCLUSIONS

This study reported superlubricious behavior obtained for a combination of $Ti_3C_2T_x$ and MoS_2. The friction results shown here have been observed to be the lowest values reported in the published literature despite testing at very high contact pressures, exceeding 1 GPa. This was explained based on extensive mechanical, microstructural, and molecular-bonding

https://doi.org/10.1021/acsnano.2c09640
ACS Nano 2023, 17, 2421−2430

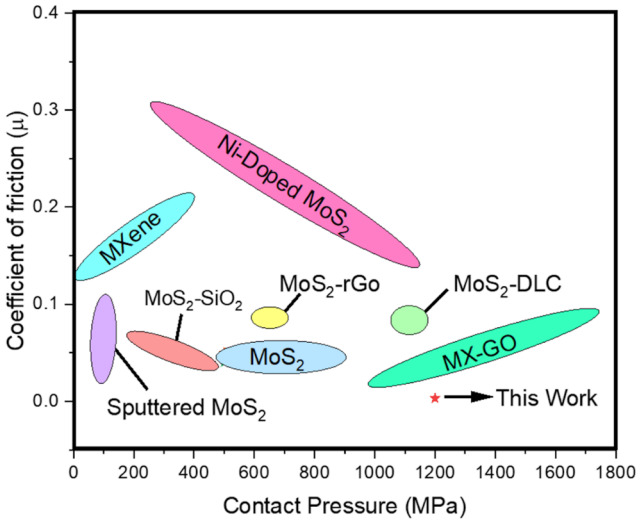

Figure 6. Ashby plot showing friction on the *y* axis and contact pressure on the *x* axis for various MoS_2 and MXene materials under pristine and blended/doped conditions juxtaposed with current results.

features of MoS_2 and MXenes, originating from the reorientation of MoS_2 basal planes and a MXene truss supporting the tribolayer all the while retaining the crystallographic integrity of the two materials at high contact pressures and sliding at high velocities. This template of materials development is hoped to accelerate the adoption of solid lubricants onto rough surfaces and translate into commercial applications as well as develop material combinations with even better properties.

METHODS

Materials. To generate accordion-like multilayer $Ti_3C_2T_x$ nanosheets, 2 g of MAX-Ti_3AlC_2 in powder form (Forsman Scientific Co. Ltd., Beijing, China) was treated with 40% hydrofluoric acid. The etching steps consisted of magnetic stirring at 60 rpm at 35 °C for 24 h. The suspension was centrifuged at 3500 rpm for 5 min, and the residual product was collected. The final pH of 6 was adjusted by several washing cycles with deionized water. Subsequently, the suspension was vacuum-filtered and freeze-dried for 24 h at −60 °C and a pressure of <30 Pa. Multilayer microcrystalline MoS_2 flakes were purchased from Graphene Supermarket, NY, USA.

Coating Preparation. The coatings were prepared using multilayer $Ti_3C_2T_x$ and MoS_2 suspended in ethyl alcohol. For these blends, 6 mg of MoS_2 was mixed with 6 mL of ethanol and 25 μL of a $Ti_3C_2T_x$ suspension (concentration 70 mg/mL). The solution was mixed thoroughly to create a multilayer $Ti_3C_2T_x$-MoS_2 blend. The prepared solution was sonicated for 5 min, such that the solution was thoroughly mixed and ready for deposition. This solid lubricant alcohol suspension was then transferred into the holding cup of a pneumatic spray deposition apparatus. Dry nitrogen was used to prevent any oxidation or deleterious intercalation during spray coating. The 50 mm in diameter test coupons were made of hardened and tempered AISI 52100 having a hardness of 59 ± 1 HR_C and roughness R_a of 250 ± 50 nm. The substrate was heated to 90 ± 10 °C to accelerate the evaporation of the carrier solution, instantaneously depositing the contained solids onto the substrates. Special care was taken not to change the properties of the base steel through tempering by limiting the thermal cycle to less than 20 min and maintaining subtempering temperatures.

Tribological Analysis. Following the preparation of substrates, the friction and wear response were evaluated under a dry nitrogen atmosphere (−44 °C dew point under continuous purging) using an Anton Paar tribometer under unidirectional sliding against AISI 52100 steel counterface spheres (6 mm diameter with a hardness of 57 HR_C and R_a = 60 ± 2 nm). A schematic of creating the suspension, spray coating, and tribological tests is shown in Figure 1. Tests were carried out at 1 N (Hertzian contact pressure ∼480 MPa), 3 N (∼690 MPa), 5 N (∼820 MPa), 10 N (∼1000 MPa), and 20 N (∼1130 MPa) with sliding at 0.2 m/s linear speeds and run at the same linear distance. Endurance tests were conducted for 2 h (equal to a distance of 1.2 km or 40k cycles) at promising test parameters to assess the longevity of the hybrid coatings. For comparison and benchmarking, steel-against-steel tests were run at 20 N under dry nitrogen.

Characterization. Optical profilometry was used to measure the coating thickness prior to the onset of experiments as well as the respective wear loss on the tribopairs after the tests. The morphologies of the as-received nanosheets, coated substrates, and formed tribolayer were studied using scanning electron microscopy (FEI Quanta 200 SEM equipped with energy-dispersive X-ray spectroscopy (EDS) at 5 kV beam voltage), transmission electron microscopy (JEOL 2000F), and optical microscopy (Leica optical microscope). Chemical changes in the coatings were recorded using Raman spectroscopy (Renishaw Raman system with a green 532 nm wavelength laser) and X-ray photoelectron spectroscopy (PHI Versaprobe, Al Kα radiation). The mechanical response was recorded using a KLA iNano nanoindenter with a diamond Berkovich tip at 10000 mN load in a continuous sensing mode. A Filmetrics Profilm3D Optical Profilometer from KLA Instruments (Milpitas, California) was used to generate the 2D and 3D surface profiles of sample surfaces.

ASSOCIATED CONTENT

Data Availability Statement

The authors confirm that the data supporting the findings of this study are available within the article.

Supporting Information

The Supporting Information is available free of charge at https://pubs.acs.org/doi/10.1021/acsnano.2c09640.

The coating optimization procedure and material analysis, friction analysis of the single-component coatings, optical images of wear tracks, characterization of the counterface, Raman analysis of the weartrack formed during sliding in A humid environment, and XPS and ED analyses (PDF)

AUTHOR INFORMATION

Corresponding Authors

Diana Berman − *Department of Materials Science and Engineering, The University of North Texas, Denton, Texas 76203, United States;* orcid.org/0000-0002-9320-9772; Email: Diana.Berman@unt.edu

Aditya Ayyagari − *Department of Materials Science and Engineering, The University of North Texas, Denton, Texas 76203, United States*; Email: Aditya.Ayyagari@unt.edu

Authors

Ali Macknojia − *Department of Materials Science and Engineering, The University of North Texas, Denton, Texas 76203, United States*

Dario Zambrano − *Department of Chemical Engineering, Biotechnology and Materials (FCFM), University of Chile, Santiago 8370456, Chile;* orcid.org/0000-0002-3484-4784

Andreas Rosenkranz − *Department of Chemical Engineering, Biotechnology and Materials (FCFM), University of Chile, Santiago 8370456, Chile;* orcid.org/0000-0002-9006-1127

Elena V. Shevchenko − *Center for Nanoscale Materials, Argonne National Laboratory, Argonne, Illinois 60439, United States; Department of Chemistry and James Frank Institute, University of Chicago, Chicago, Illinois 60637, United States;* orcid.org/0000-0002-5565-2060

Complete contact information is available at: https://pubs.acs.org/10.1021/acsnano.2c09640

Notes

The authors declare no competing financial interest.

ACKNOWLEDGMENTS

The authors acknowledge the support of this work by the National Science Foundation (NSF) (Award No. 2018132). A.R. acknowledges the financial support given by ANID-Chile within the projects Fondequip EQM190057, Fondecyt Regular 1220331, and Fondecyt Postdoctorado 3220165. Work performed at the Center for Nanoscale Materials, a U.S. Department of Energy Office of Science User Facility, was supported by the U.S. DOE, Office of Basic Energy Sciences, under Contract No. DE-AC02-06CH11357.

REFERENCES

(1) Ayyagari, A.; Alam, K. I.; Berman, D.; Erdemir, A. Progress in Superlubricity Across Different Media and Material Systems - A Review. *Front. Mech. Eng.* **2022**, *8*, 908497.

(2) Kawai, S.; Benassi, A.; Gnecco, E.; Söde, H.; Pawlak, R.; Feng, X.; Müllen, K.; Passerone, D.; Pignedoli, C. A.; Ruffieux, P.; Fasel, R.; Meyer, E. Superlubricity of graphene nanoribbons on gold surfaces. *Science.* **2016**, *351*, 957−961.

(3) Sinclair, R. C.; Suter, J. L.; Coveney, P. V. Graphene-Graphene Interactions: Friction, Superlubricity, and Exfoliation. *Adv. Mater.* **2018**, *30*, 1705791.

(4) Liu, S.; Wang, H.; Xu, Q.; Ma, T.; Yu, G.; Zhang, C.; Geng, D.; Yu, Z.; Zhang, S.; Wang, W.; Hu, Y. Z.; Wang, H.; Luo, J. Robust microscale superlubricity under high contact pressure enabled by graphene-coated microsphere. *Nat. Commun.* **2017**, *8*, 14029.

(5) Leven, I.; Krepel, D.; Shemesh, O.; Hod, O. Robust Superlubricity in Graphene/h-BN Heterojunctions. *J. Phys. Chem. Lett.* **2013**, *4*, 115−120.

(6) Li, J.; Lil, J.; Luo, J. Superlubricity of Graphite Sliding against Graphene Nanoflake under Ultrahigh Contact Pressure. *Adv. Sci.* **2018**, *5*, 1800810.

(7) Berman, D.; Deshmukh, S. A.; Sankaranarayanan, S. K. R. S.; Erdemir, A.; Sumant, A. V. Macroscale superlubricity enabled by graphene nanoscroll formation. *Science.* **2015**, *348*, 1118−1122.

(8) Huang, P.; Qia, W.; Yina, X.; Choi, J.; Chena, X.; Tiana, J.; Xua, J.; Wub, H.; Luo, J. Ultra-low friction of a-C:H films enabled by lubrication of nanodiamond and graphene in ambient air. *Carbon.* **2019**, *154*, 203−210.

(9) Jiang, B.; Zhao, Z.; Gong, Z.; Wang, D.; Yu, G.; Zhang, J. Superlubricity of metal-metal interface enabled by graphene and $MoWS_4$ nanosheets. *Appl. Surf. Sci.* **2020**, *520*, 146303.

(10) Mutyala, K. C.; Doll, G. L.; Wen, J.; Sumant, A. V. Superlubricity in rolling/sliding contacts. *Appl. Phys. Lett.* **2019**, *115*, 103103.

(11) Berman, D.; Erdemir, A.; Sumant, A. Approaches for Achieving Superlubricity in Two-Dimensional Materials. *ACS Nano* **2018**, *12*, 2122−2137.

(12) Martin, J. M.; Pascala, H.; Donnet, C.; Mogne, T. L.; Loubet, J. L.; Epicier, T. Superlubricity of MoS_2: crystal orientation mechanisms. *Surf. Coat. Technol.* **1994**, *68−69*, 427−432.

(13) Mogne, T. L.; Donnet, C.; Martin, J. M. Nature of super-lubricating MoS2 physical vapor deposition coatings. *J. Vac. Sci. Technol. A* **1994**, *12*, 1998−2004.

(14) Marian, M.; Berman, D.; Rota, A.; Jackson, R. L.; Rosenkranz, A. Layered 2D Nanomaterials to Tailor Friction and Wear in Machine Elements—A Review. *Adv. Mater. Interface* **2022**, *9*, 2101622.

(15) Liu, Z.; Yang, J.; Grey, F.; Liu, J. Z.; Liu, Y.; Wang, Y.; Yang, Y.; Cheng, Y.; Zheng, Q. Observation of Microscale Superlubricity in Graphite. *Phys. Rev. Lett.* **2012**, *108*, 205503.

(16) Nine, M. J.; Cole, M. A.; Trana, D. N. H.; Losic, D. Graphene: a multipurpose material for protective coatings. *J. of Mater. Chem. A* **2015**, *3*, 12580−12602.

(17) Donnet, C.; Mogne, T. L.; Martin, J. M. Superlow friction of oxygen-free MoS_2 coatings in ultrahigh vacuum. *Surf. Coat. Technol.* **1993**, *62*, 406−411.

(18) Berman, D.; Erdemir, A.; Sumant, A. Few layer graphene to reduce wear and friction on sliding steel surfaces. *Carbon.* **2013**, *54*, 454−459.

(19) Berman, D.; Erdemir, A.; Zinovev, A.; Sumant, A. Nanoscale friction properties of graphene and graphene oxide. *Diamond Relat. Mater.* **2015**, *54*, 91−96.

(20) Hao, R.; Tedstone, A. A.; Lewis, D. J.; Warrens, C. P.; West, K. R.; Howard, P.; Gaemers, S.; Dillon, S. J.; O'Brien, P. Property Self-Optimization During Wear of MoS_2. *ACS Appl. Mater. Interfaces.* **2017**, *9*, 1953−1958.

(21) Simmonds, M.; Savan, A.; Pflüger, E.; Swygenhoven, H. V. Mechanical and tribological performance of MoS_2 co-sputtered composites. *Surf. Coat. Technol.* **2000**, *126*, 15−24.

(22) Andrew, J. M. Expanding the repertoire of solid lubricant MoS_2. *Tribol. Lubr. Technol.* **2021**, *77*, 40−42.

(23) Kumari, S.; Chouhan, A.; Sharma, O. P.; Tawfik, S. A.; Tran, K.; Spencer, M. J.; Bhargava, S. K.; Walia, S.; Ray, A.; Khatri, O. P. Surface Functionalization of WS_2 Nanosheets with Alkyl Chains for Enhancement of Dispersion Stability and Tribological Properties. *ACS Appl. Mater. Interfaces.* **2022**, *14*, 1334−1346.

(24) Lian, Y.; Deng, J.; Yan, G.; Cheng, H.; Zhao, J. Preparation of tungsten disulfide (WS_2) soft-coated nano-textured self-lubricating tool and its cutting performance. *Int. J. Adv. Manuf. Technol.* **2013**, *68*, 2033−2042.

(25) Vadiraj, A.; Kamaraj, M. Comparative Wear Behavior of MoS_2 and WS_2 Coating on Plasma-Nitrided SG iron. *J. Mater. Eng. Perform.* **2010**, *19*, 166−170.

(26) Lian, Y.; Deng, J.; Li, S.; Xing, Y.; Chen, Y. Preparation and cutting performance of WS2 soft-coated tools. *Int. J. Adv. Manuf. Technol.* **2013**, *67*, 1027−1033.

(27) Ayyagari, A. V.; Mutyala, K. C.; Sumant, A. V. Towards developing robust solid lubricant operable in multifarious environments. *Sci. Rep.* **2020**, *10*, 1−12.

(28) Curry, J. F. *Friction and Environmental Sensitivity of Molybdenum Disulfide: Effects of Microstructure*, Theses and Dissertations; Lehigh University: 2017.

(29) Khare, H. S.; Burris, D. Surface and subsurface contributions of oxidation and moisture to room temperature friction of molybdenum disulfide. *Trib. Lett.* **2014**, *53*, 329−336.

(30) Khare, H. S.; Burris, D. The Effects of Environmental Water and Oxygen on the Temperature-Dependent Friction of Sputtered Molybdenum Disulfide. *Trib. Lett.* **2013**, *52*, 485−493.

(31) Gao, K.; Wang, B.; Shirani, A.; Chang, Q.; Berman, D. Macroscale Superlubricity Accomplished by Sb_2O_3-MSH/C Under High Temperature. *Front. Chem.* **2021**, *9*, 667878.

(32) Yin, X.; Jin, J.; Chen, X.; Rosenkranz, A.; Luo, J. Ultra-wear-resistant MXene-based composite coating via in situ formed nanostructured tribofilm. *ACS Appl. Mater. Interfaces.* **2019**, *11*, 32569−32576.

(33) Marian, M.; Tremmel, S.; Wartzack, S.; Song, G.; Wang, B.; Yu, J.; Rosenkranz, A. MXene nanosheets as an emerging solid lubricant for machine elements - Towards increased energy efficiency and service life. *Appl. Surf. Sci.* **2020**, *523*, 146503.

(34) Gao, J.; Du, C. F.; Zhang, T.; Zhang, X.; Ye, Q.; Liu, S.; Liu, W. Dialkyl Dithiophosphate-Functionalized $Ti_3C_2T_x$ MXene Nanosheets as Effective Lubricant Additives for Antifear and Friction Reduction. *ACS Appl, Nano Mater.* **2021**, *4*, 11080−11087.

(35) Yi, S.; Guo, Y.; Li, J.; Zhang, Y.; Zhou, A.; Luo, J. Two-dimensional molybdenum carbide (MXene) as an efficient nano-additive for achieving superlubricity under ultrahigh pressure. *Friction* **2023**, *11*, 369−382.
(36) Yi, S.; Li, J.; Liu, Y.; Ge, X.; Zhang, J.; Luo, J. In-situ formation of tribofilm with $Ti_3C_2T_x$ MXene nanoflakes triggers macroscale superlubricity. *Tribol. Int.* **2021**, *154*, 106695.
(37) Tian, P.; Yuc, G.; Wei, K.; Zhang, Z.; Wanga, N. Effect of hydroxyl intercalation on tribological properties of MXene ($Ti_3C_2T_x$). *Ceram. Int.* **2021**, *47*, 30722−30728.
(38) Yang, Y.; Zhu, J.; Hou, K.; Ma, L.; Li, Z.; Jia, W.; Wang, H.; Wang, J.; Yang, S. Friction-induced construction of PTFE-anchored MXene heterogeneous lubricating coating and its in-situ tribological transfer mechanism. *J. Chem. Eng.* **2022**, *442*, 136238.
(39) Zhang, H.; Wang, L.; Chen, Q.; Li, P.; Zhou, A.; Cao, X.; Hu, Q. Preparation; mechanical and anti-friction performance of MXene/polymer composites. *Mater. Des* **2016**, *92*, 682−689.
(40) Zhang, H.; Wang, L.; Zhou, A.; Shen, C.; Dai, Y.; Liu, F.; Chen, J.; Li, P.; Hua, Q. Effects of 2-D transition metal carbide Ti_2CT_x on properties of epoxy composites. *RSC Adv.* **2016**, *6*, 87341−87352.
(41) Carey, M.; Barsoum, M. W. MXene polymer nanocomposites: a review. *Mater. Today Adv.* **2021**, *9*, 100120.
(42) Jimmy, J.; Kandasubramanian, B. Mxene functionalized polymer composites: Synthesis and applications. *Eur. Polym. J.* **2020**, *122*, 109367.
(43) Rosenkranz, A.; Grützmacher, P. G.; Espinoza, R.; Fuenzalida, V. M.; Blanco, E.; Escalona, N.; Garica, F. J.; Villarroeal, R.; Guo, L.; Kang, R.; Mücklich, F.; Suarez, S.; Zhang, Z. Multi-layer Ti3C2Tx-nanoparticles (MXenes) as solid lubricants - Role of surface terminations and intercalated water. *Appl. Surf. Sci.* **2019**, *494*, 13−21.
(44) Marian, M.; Song, G. C.; Wang, B.; Fuenzalida, V. M.; Krauß, S.; Merle, B.; Tremmel, S.; Wartzack, S.; Yu, J.; Rosenkranz, A. Effective usage of 2D MXene nanosheets as solid lubricant - Influence of contact pressure and relative humidity. *Appl. Surf. Sci.* **2020**, *531*, 147311.
(45) Mai, Y. J.; Li, Y. G.; Li, S. L.; Zhang, L. Y.; Liu, C. S.; Jie, X. H. Self-lubricating Ti_3C_2 nanosheets/copper composite coatings. *J. Alloys Compd.* **2019**, *770*, 1−5.
(46) Guan, H.; Lu, X.; Yao, Q.; Wang, Y.; Liu, X.; Xia, G.; Zhao, D. Microstructure and tribological behavior of $Ti_3C_2T_x$ MXene reinforced chemically bonded silicate ceramic coatings. *Ceram. Int.* **2022**, *48*, 1926−1935.
(47) Liu, F.; Liul, F.; Zhang, R.; Chen, X. Microstructure and tribological property of a MXene derived from Ti_3AlC_2. *Mater. Res. Express.* **2022**, *9*, 025004.
(48) Huang, S.; Mutyala, K. C.; Mochalin, V. N. Achieving superlubricity with 2D transition metal carbides (MXenes) and MXene/graphene coatings. *Mater. Today.* **2021**, *9*, 100133.
(49) Windom, B. C.; Sawyer, W. G.; Hahn, D. W. A Raman Spectroscopic Study of MoS_2 and MoO_3: Applications to Tribological Systems. *Tribol. Letters.* **2011**, *42*, 301−310.
(50) Szoszkiewicz, R. Local Interactions of Atmospheric Oxygen with MoS2 Crystal. *Materials.* **2021**, *14*, 5979.
(51) Spalvins, T. A review of recent advances in solid film lubrication. *J. Vac. Sci. Technol. A* **1987**, *5*, 212.
(52) Singer, I. L.; Bolster, R. N.; Wegand, J.; Fayeulle, S.; Stupp, B. C. Hertzian stress contribution to low friction behavior of thin MoS2 coatings. *Appl. Phys. Lett.* **1990**, *57*, 995.
(53) Xin, Y.; Li, T.; Gong, D.; Xu, F.; Wang, M. Preparation and tribological properties of graphene oxide/nano-MoS_2 hybrid as multidimensional assembly used in polyamide nanocomposites. *RSC Adv.* **2017**, *7*, 6323−6335.
(54) Zhao, J.; He, Y.; Wang, Y.; Wang, W.; Yan, L.; Luo, J. An investigation on the tribological properties of multilayer graphene. *Tribol. Int.* **2016**, *97*, 14−20.
(55) Panitz, J. K. G.; Pope, L. E.; Lyons, J. E.; Staley, D. J. The tribological properties of MoS_2 coatings in vacuum, low relative humidity. *J. Vac. Sci. Technol.* **1988**, *6*, 1166−1170.
(56) He, D.; Cai, M.; Yan, H.; Lina, Q.; Fan, X.; Zhang, L.; Zhu, M. Tribological properties of $Ti_3C_2T_x$ MXene reinforced interpenetrating polymers network coating. *Tribol. Int.* **2021**, *163*, 107196.
(57) Qu, C.; Li, S.; Zhang, Y.; Wang, T.; Wang, Q.; Chen, S. Surface modification of Ti_3C_2-MXene with polydopamine and amino silane for high performance nitrile butadiene rubber composites. *Tribol. Int.* **2021**, *163*, 107150.

https://doi.org/10.1021/acsnano.2c09640
ACS Nano 2023, 17, 2421−2430